

On-chip visible light communication-band metasurface modulators with niobium plasmonic nano-antenna arrays

Kaveh Delfanazari ^{1,*} & Otto L. Muskens ²

1. James Watt School of Engineering, University of Glasgow, Glasgow G12 8QQ, UK

2. Physics and Astronomy, University of Southampton, Southampton SO17 1BJ, UK

*corresponding author: kaveh.delfanazari@glasgow.ac.uk

Dated: 20072021

We introduce chip-integrated visible light communication-band modulators based on niobium (Nb) metallic plasmonic nano-antenna arrays. Our plasmonic nano-devices provide strong sensitivity to the polarization of the incident visible light and the geometrical parameters of their subwavelength nanoscale building blocks. Moreover, they offer optical modulation properties with modulation depth $MD \cong 60\%$ at resonant wavelength $\lambda = 716$ nm, at room temperature. By engineering the photo response of the Nb nano-device arrays, we observe a maximum extinction $A(\lambda) = 1 - R(\lambda) \cong 95\%$ at resonant wavelength $\lambda = 650$ nm. Our results suggest that the integrated Nb nano-antenna array devices can be considered as suitable platforms for the realisation of chip-scale optoelectronic devices interfacing cryogenics quantum circuits, and fibre-based communication systems, for applications in quantum computing, quantum communication, and quantum processing.

Niobium (Nb), a metallic superconductor with quantum mechanics phases below their superconducting transition temperature $T_c \cong 9$ K, has been widely used in superconducting quantum technology. Superconducting quantum circuits have shown potential as a leading technology for quantum computing [1-10]. Cryogenic photonic links using optical fibres with their low thermal conductivity have been recently introduced to surpass the heat load associated with the growing number of quantum processors in low temperatures and to connect superconducting quantum hardware nodes with fibre-based telecommunication platforms [6-8]. Nevertheless, the optical properties of superconducting circuits, superconducting nanostructures, and the devices interfacing superconductors and photonics are surprisingly unexplored [6-10]. Here, at the first step, the photo-response of niobium (Nb) nano-antenna arrays of different geometries is studied both numerically (using COMSOL Multiphysics) and experimentally (using a microspectrophotometer CRAIC QDI2010, and an ultrafast laser with pulse duration 400 fs) at room temperature.

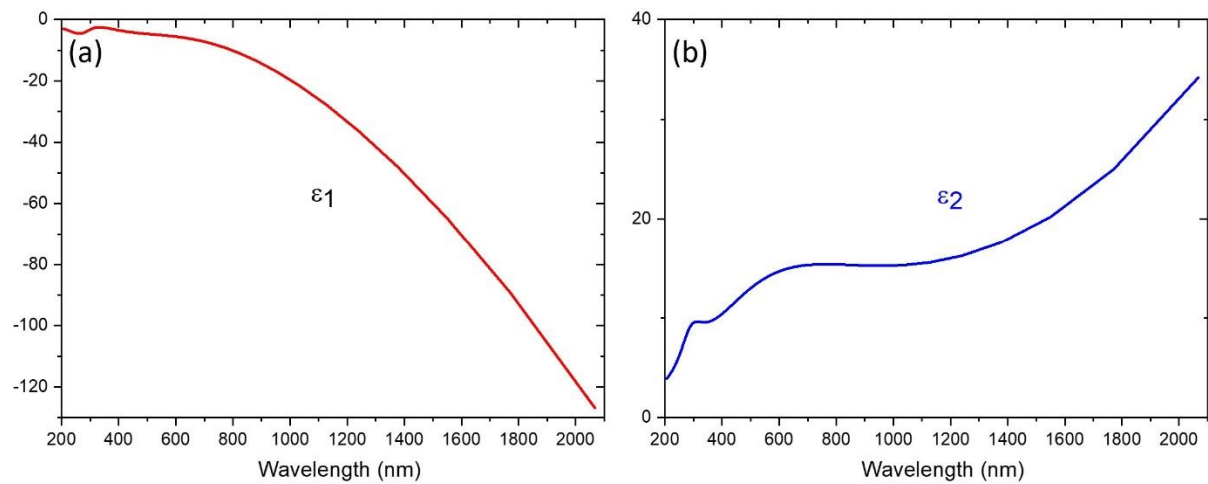


Figure 1: the dielectric function of the unstructured Nb film at room temperature, measured by variable-angle spectroscopic ellipsometry in the visible and optical light communication frequencies. Plasmonic property of Nb is shown for a broad frequency range.

To fabricate the integrated nano-devices, Nb thin film of 300 nm thickness was sputtered onto a sapphire substrate of 30 mm diameter and 0.5 mm thickness. To explore the optical properties of unstructured Nb thin film and to be able to simulate the photoresponse of our nano-devices

in COMSOL, the variable-angle spectroscopic ellipsometry measurement was performed in the wavelengths ranges from $\lambda = 200$ nm to 2000 nm at room temperature and down to liquid nitrogen temperature (not shown here) using a Horiba Uvisel-2 spectroscopic ellipsometer [9]. Figure 1 shows the Nb plasmonic properties and a negative permittivity which was observed from UV to NIR frequency ranges. The superconducting transition temperature T_c of our unstructured Nb thin films was confirmed to be around $T_c \cong 9$ K through the DC transport measurements (not shown here). The integrated nano-antenna arrays were patterned by focused ion beam milling FIB (FEI Helios NanoLab 600). In total, we fabricated five chips, each with an array of Nb subwavelength elements of different geometries, each array covering a total area of $100 \times 100 \mu\text{m}^2$. The light-matter interaction experiments were done when the Nb chip was loaded in closed-cycle optical cryostats with temperature tuning range capability between $T = 293$ K and 3 K.

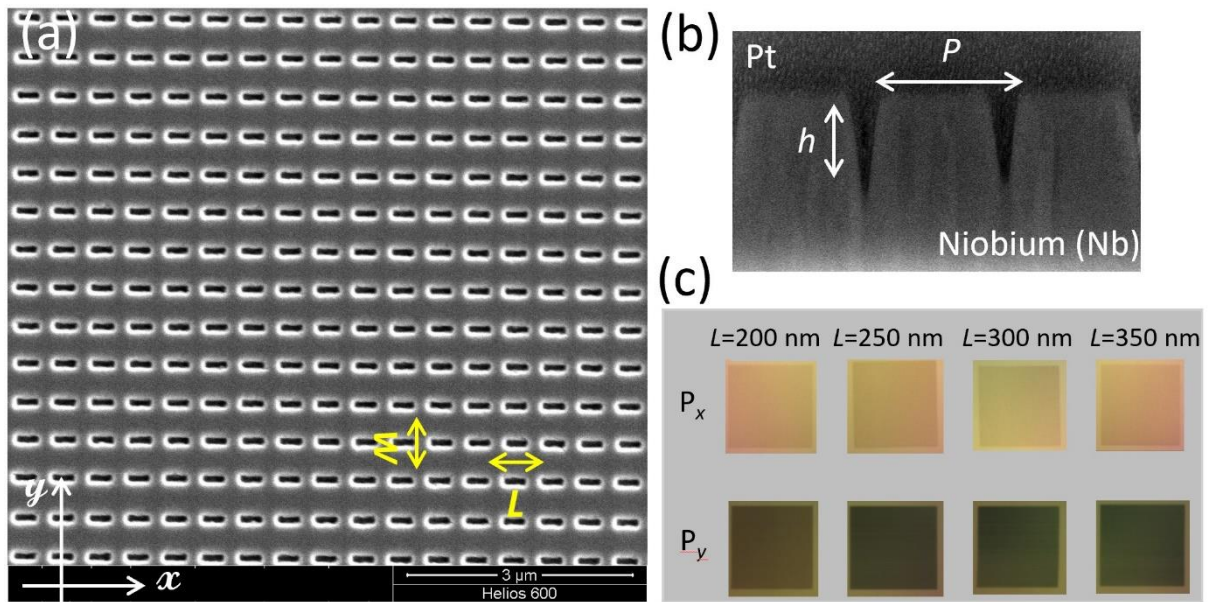


Figure 2: (a) Scanning Electron Microscope (SEM) image of the Nb integrated nanocircuitry with superconducting transition temperature $T_c \cong 9$ K. (b) SEM of the cross section of the part of the Nb nano-antenna array showing the antenna profile with a period $P \cong 500$ nm and a depth $h \cong 200$ nm. Platinum (Pt) layer was deposited, after optical spectroscopy, for protection during sectioning for device characterisation purposes. (c) optical microscope image of four chips with arrays of plasmonic Nb nano-antennas at two different polarization angles. Plasmonic colours for the optical nano-antenna arrays depends on the meta-atom geometrical parameters, and the angle of the incident light.

We first present the data for four chips that contain an array of nano-antennas of rectangle (slit) geometries. In the chips, the slit lengths vary between $L \cong 200$ nm, 250 nm, 300 nm, and 350 nm for a fixed width $w \cong 50$ nm. Figure 2 (a) illustrates an example of the integrated nano-device fabricated by using FIB. Figure 2 (b) shows the SEM image of the cross-section of part of the array. The optical nano-antenna array has a period of $P \cong 500$ nm and a depth of $h \cong 200$ nm. The platinum (Pt) layer was deposited, after optical spectroscopy, for protection during sectioning for device characterization purposes. The nano-antenna arrays provide plasmonic colors when illuminated with white light. Figure 2 (c) shows the optical microscope images of four chips with collections of plasmonic Nb nano-antenna arrays at incident light polarizations parallel (P_x) and perpendicular (P_y) to the slits. Plasmonic colors for the optical nano-antenna arrays change with each meta-atom length and with the incident light polarization.

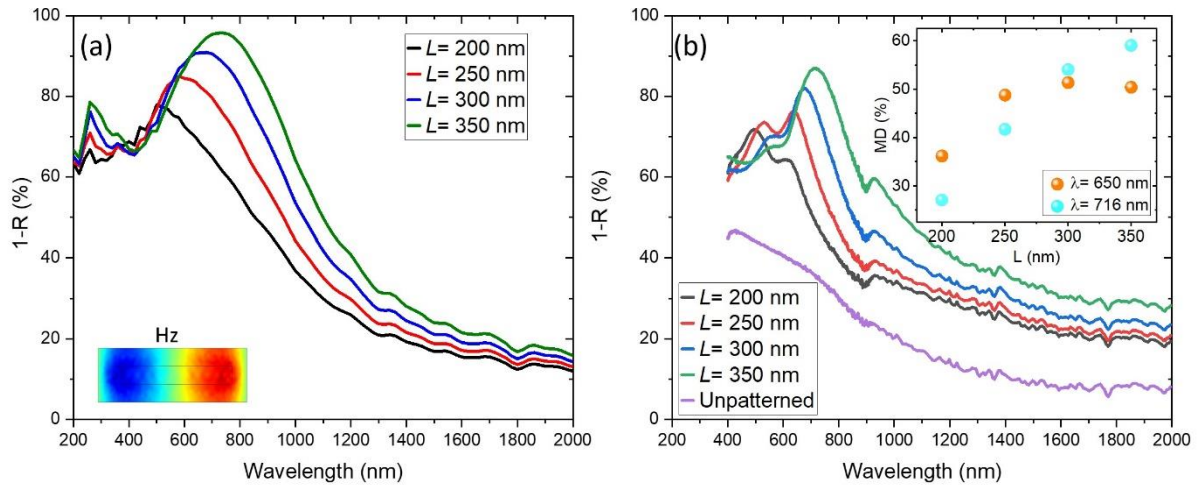


Figure 3: (a) The numerical simulation, and (b) experimental resonant response of various nano-antenna arrays with length varying from $L = 200$ nm to 350 nm for light polarized perpendicular to the slits (P_y). Inset to Fig. 3 (a) is the H_z -field distribution in the nano-antenna at the resonance wavelength $\lambda = 650$ nm.

The optical Nb nano-devices were numerically modeled using a fully three-dimensional finite element technique (COMSOL Multiphysics). The simulation results for four chips are shown in Figure 3 (a) for y -polarized plane waves (P_y). The H_z -field distribution in the nano-antenna at the resonance wavelength $\lambda = 650$ nm is shown in the inset. The resonance shows an

electrical dipole response in the field distribution in the groove. Figure 3 (b) shows the experimental results for nano-devices that were measured in a microspectrophotometer under light polarized perpendicular to the slits (P_y). We observe extinction spectra $A(\lambda)=1- R(\lambda)$ at visible light communication bands, and the resonances are found to move to longer wavelengths (redshift) with increasing nano-antenna length. Relatively good agreement can be seen between the experiment and simulation, taking into account the V-shaped profile cross-section of the nano-antennas made by FIB. A clear modulation of visible light extinction spectra could therefore be observed in Nb nano-devices by engineering the meta-atom geometrical parameters.

The modulation depth (MD) is defined as [11,12]

$$MD = \frac{A_{Nb \text{ nanoantenna array}} - A_{unpatterened Nb \text{ film}}}{A_{Nb \text{ nanoantenna array}}}$$

where $A_{unpatterened Nb \text{ film}}$ and $A_{Nb \text{ nanoantenna array}}$ are maximum extinction of the unpatterned Nb thin film, and Nb nano-antenna arrays with length varying from $L=200$ nm to 350 nm, respectively. We find an apparent increase of MD with increasing the length of nano-antenna arrays. MD for $L=350$ nm, reaches the maximum value of 60 % at the resonant wavelengths $\lambda=716$ nm.

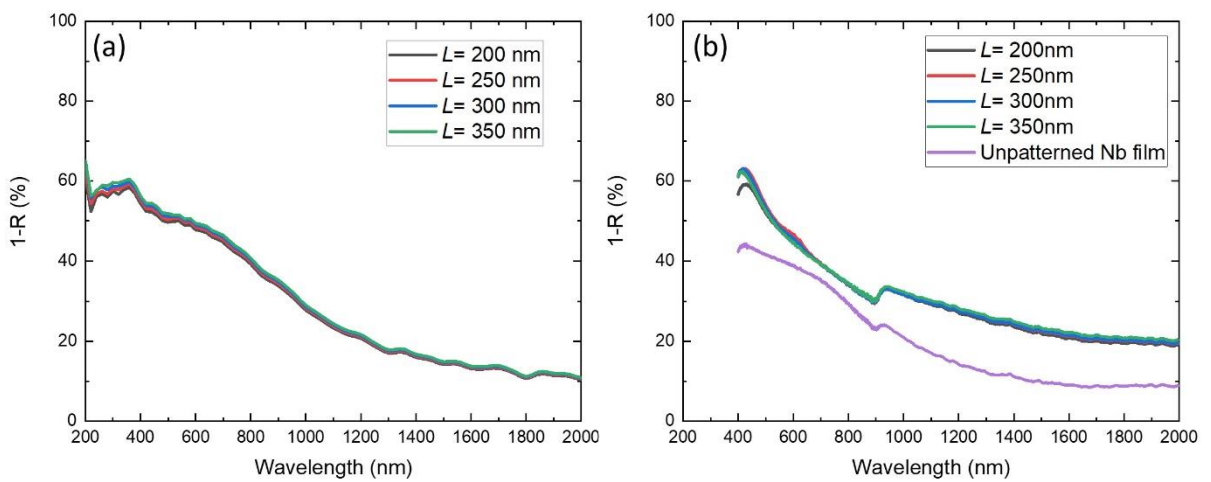


Figure 4: (a) The numerical simulation, and (b) experimental resonant response of various nanocircuit arrays with length varying from $L=200$ nm to 350 nm for light polarized parallel to the slits, (P_x).

We find that the extinction spectra $A(\lambda)=1-R(\lambda)$ are pretty different between unstructured (un-patterned) Nb thin film and nano-antenna arrays for incident light polarization perpendicular to the slits (P_y). We did not observe any resonance peaks from un-patterned Nb thin film (see Fig. 3 (b)), indicating the importance of nanostructure arrays engraved into the surface of Nb thin film in modulation and enhancement of light-matter interactions. The relatively narrow plasmon resonances that are modulated by nano-antenna arrays length of $L=200$ nm to 350 nm, for light polarized perpendicular to the slits, radically change the optical response of Nb thin film and their corresponding plasmonic colors in the visible range without a requirement to chemical modification or usage of a secondary material coating, as shown in Fig. 2 (c).

The numerical simulation and experimental measurement of the Nb nano-antenna array for light polarized parallel to the slits (P_x) are presented in Fig. 4. We find a good agreement between simulation and experimental results. The $A(\lambda)$ spectra for Nb nano-antenna arrays show a strong sensitivity to the polarization of incident light, while the photoresponse is quite small for unstructured Nb thin film. This again confirms the vital role of plasmonic nanostructures in engineering the light-matter interactions in photonic nano-circuitry.

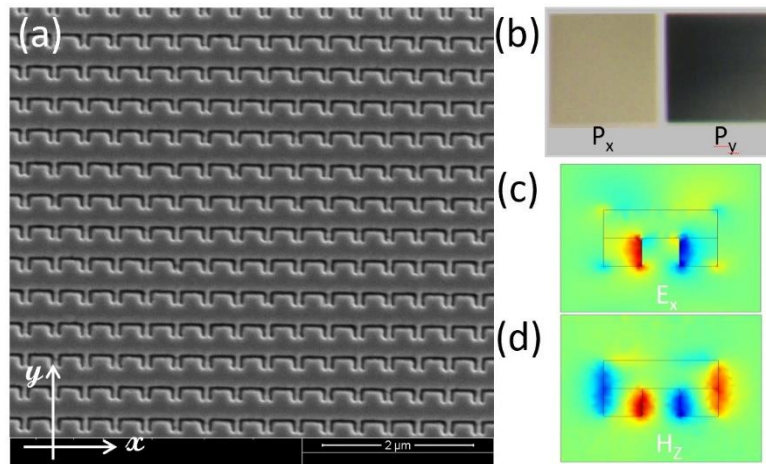


Figure 5: (a) SEM image of the Nb integrated plasmonic nano-antennas with SRR geometries. (b) optical microscope image of the arrays of plasmonic Nb nano-antennas at two different polarization, parallel (P_x) and perpendicular (P_y) to the device plane. Plasmonic colors in structured Nb films show a strong sensitivity to the geometry of the nano-antenna element and to the polarization of the incident light. Nearfield profiles of electric (c) and magnetic (d) modes at wavelength $\lambda=650$ nm.

To further investigate the effect of geometrical parameters on visible light modulation properties of Nb plasmonic nanostructures, the fifth chip was patterned with a nano-antenna array whose cavity shape is selected to be a U-Shape split-ring resonator (SRR). The chip was milled by FIB into the Nb film surface, and the high fabrication quality and uniformity of the samples were confirmed by SEM images as shown in Fig. 5 (a). Plasmonic colors of the arrays are shown in Fig. 5 (b) for two different polarizations. Similar to nano-slit antenna arrays, they show a dramatic change in color compared to that of the unstructured Nb metal thin films. The chip was loaded into an optical cryostat and measured with a microspectrophotometer at room temperature. The experimental results for light polarized parallel (P_x) and perpendicular (P_y) to the split ring resonator are presented in Fig. 6. A huge difference was found between the extinction spectra $A(\lambda)=1-R(\lambda)$ of unstructured Nb thin film (Fig. 6 (a)) and the nano-split ring resonator arrays (Fig. 6 (b)). The resonance response of the plasmonic Nb nano-split ring resonators is clearly a strong function of the geometry and size of the meta-atoms.

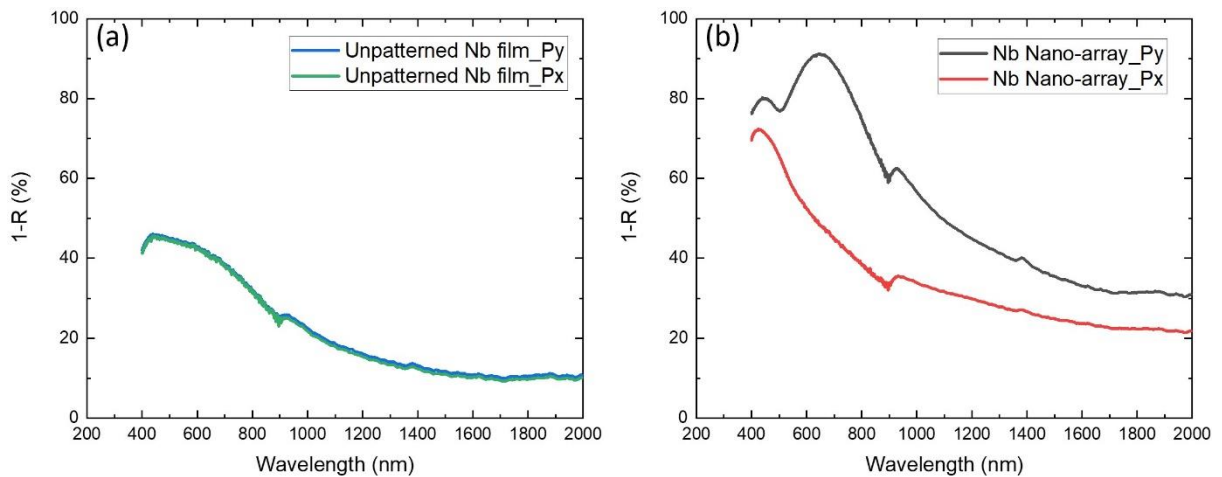


Figure 6: (a) experimental resonant response of (a) unstructured Nb thin film, and (b) nano-antenna split ring resonator array for light polarized perpendicular (P_y) and parallel (P_x) to the device plane.

Nb nano-split ring resonators contain both electric and magnetic modes. The simulated nearfield profiles of magnetic and electric modes of the nano-SRR with a U-shaped hole structure milled through the Nb metallic thin film are shown in Fig. 5 (c) and Fig. 5 (d),

respectively. The parallel dipoles in the figure indicating plasmon mode. There is no induced dipole that can be seen along the top arm of the SRR, and the H_z field is only localized around the side arms because the same charge polarity is stimulated on the Nb nano-antenna sidearms [13,14]. Robust localization of E_y -field in the Nb nano-antenna element indicates that plasmon mode is dominated by vertical dipoles. This suggests that plasmon mode in the Nb nano-antenna split ring resonator array can only be excited when the incident light is P_y polarized [13-15].

We also find that the nano-split ring resonator array chip offers a very sensitive photoresponse to the incident light polarization. We observe nearly 80% of visible light absorbance for a wide wavelength ranges between $\lambda= 400$ nm and 800 nm, which corresponds to visible light communication band, while this value reduces by more than 40 % for unstructured Nb thin film in the same wavelengths, as shown in Fig. 6. The nano-device shows a resonance peak at $\lambda= 650$ nm, with > 90 % light absorbance, make it an excellent ingredient for integration with Nb-based superconducting quantum hardware, and visible light communication system elements, such as polymer optical fibre (POF) with their robustness under bending and stretching. Nb photonic nano-devices integrated with POF-based, or similar technology readout platforms with low thermal conductivity [6-8], may also help to reduce the heat load associated with the growing number of quantum hardware in cryogenic temperatures. Such plasmonic nano-devices in different geometrical parameters can also be integrated with other quantum devices, such as quantum light sources, hybrid light modulators, and slow light devices to improve their optical functionalities [16-35]. Our approach may also help the development of on-chip integrated nano-photonic circuits and devices [36-60].

Conclusion:

We fabricated plasmonic nano-antenna arrays of different geometries on the facet of Nb thin films by using FIB milling. Our Nano-device arrays offer optical modulation of light at visible

communication bands with a maximum modulation depth $MD \cong 60\%$ at resonant wavelength $\lambda = 716$ nm, at room temperature. We observe maximum extinction spectra $A(\lambda) = 1 - R(\lambda) \cong 95\%$ at wavelength $\lambda = 650$ nm by engineering the Nb nano-device arrays geometrical parameters. Metallic nanostructures based on Nb become superconductors with a quantum mechanic phase around $T = 9$ K, offering potential thermo-photo modulation of visible light at cryogenic temperatures. Such nano-devices have the potential to be integrated with Nb-based superconducting quantum hardware and fiber-based telecommunication read-out systems, paving the way for the realisation of chip-scale all superconducting photonic links, modulators, and filters for applications in quantum computing and communication.

References:

- [1] F. Arute, *et al.*, Quantum supremacy using a programmable superconducting processor, *Nature* 574, 505–510 (2019).
- [2] K. Delfanazari, *et al.*, On-Chip Andreev Devices: Hard Superconducting Gap and Quantum Transport in Ballistic Nb–In_{0.75}Ga_{0.25}As-Quantum-Well–Nb Josephson Junctions. *Adv. Mater.* 2017, 29 (37), 1701836
- [3] D. Pitsun, *et al.*, Cross Coupling of a Solid-State Qubit to an Input Signal due to Multiplexed Dispersive Readout, *Phys. Rev. Applied* 14 (5), 054059 (2020).
- [4] K. Delfanazari, *et al.*, On-Chip Hybrid Superconducting-Semiconducting Quantum Circuit. *IEEE Trans. Appl. Supercond.* 28:1100304 (2018). DOI: 10.1109/TASC.2018.2812817
- [5] K. Delfanazari, *et al.*, Scalable Quantum Integrated Circuits on Superconducting Two-Dimensional Electron Gas Platform, *J. Vis. Exp.* (150), e57818, doi:10.3791/57818 (2019).
- [6] F. Lecocq, *et al.*, Control and read-out of a superconducting qubit using a photonic link, *Nature* 591, 575–579 (2021).
- [7] K. Usami and Y. Nakamura, A photonic link for quantum circuits, *Nature Electronics* 4, May 2021, 323–324. <https://doi.org/10.1038/s41928-021-00587-9>
- [8] A. Youssefi, *et al.*, A cryogenic electro-optic interconnect for superconducting devices, *Nature Electronics*, 4, May 2021, 326-332. <https://doi.org/10.1038/s41928-021-00570-4>
- [9] K. Delfanazari, *et al.*, Light-matter interactions in chip-integrated niobium nano-circuit arrays at optical fibre communication frequencies, *arXiv:2107.03677*
- [10] L. Yang, *et al.*, Proximitized Josephson junctions in highly-doped InAs nanowires robust to optical illumination, *Nanotechnology* 32 (7), 075001 (2020).
- [11] S. Kalhor, *et al.*, Active terahertz modulator and slow light metamaterial devices with hybrid graphene-superconductor photonic integrated circuits, *arXiv: 2107.03677*.
- [12] C. Li, *et al.*, Electrical dynamic modulation of THz radiation based on superconducting metamaterials *Appl. Phys. Lett.* 111, 092601 (2017).
- [13] C. Rockstuhl, *et al.*, On the reinterpretation of resonances in split-ring-resonators at normal incidence, *Optics Express* 8827, 14, 19 (2006).
- [14] C. Enkrich, *et al.*, Magnetic Metamaterials at Telecommunication and Visible Frequencies, *Phys. Rev. Lett.* 95, 203901 (2005)
- [15] S. Kalhor, *et al.*, Millimeter wave to terahertz compact and low-loss superconducting plasmonic waveguides for cryogenic integrated nano-photonics, *arXiv:2106.08594*.
- [16] K. Delfanazari, *et al.*, Integrated, Portable, Tunable, and Coherent Terahertz Sources and Sensitive Detectors Based on Layered Superconductors. *Proc. IEEE* 2020, 108 (5), 721–734.
- [17] K. Delfanazari, *et al.*, Tunable Terahertz Emission from the Intrinsic Josephson Junctions in Acute Isosceles Triangular Bi₂Sr₂CaCu₂O_{8+δ} Mesas. *Opt. Express* 2013, 21 (2), 2171.
- [18] S. Kalhor, *et al.*, Thermal Tuning of High-Tc Superconducting Bi₂Sr₂CaCu₂O_{8+δ} Terahertz Metamaterial. *IEEE Photonics J.* 2017, 9 (5), 1–8.
- [19] K. Kadowaki, *et al.*, Terahertz wave emission from intrinsic Josephson junctions in Bi₂Sr₂CaCu₂O_{8+δ}, *J. Phys: Conf. Ser* 400 (2), 022041 (2012).

- [20] T. Kashiwagi, *et al.*, Excitation mode characteristics in Bi2212 rectangular mesa structures, *J. Phys: Conf. Ser* 400 (2), 022050 (2012).
- [21] T. Kitamura, *et al.*, Effects of magnetic fields on the coherent THz emission from mesas of single crystal Bi₂Sr₂CaCu₂O_{8+δ}, *Physica C*, 494, 117-120 (2013).
- [22] K. A. Fedorova, *et al.*, Widely Tunable Terahertz-Generating Semiconductor Disk Laser, *Phys. Status Solidi RRL* 2020, 14, 2000204.
- [23] S. Kalhor, *et al.*, Guiding of terahertz photons in superconducting nano-circuits, *2020 Int. Conf. UK-China Emerg. Technol. UCET 2020* 2020, 1-3, doi:10.1109/UCET51115.2020.9205480.
- [24] T. Kashiwagi, *et al.*, High temperature superconductor terahertz emitters: fundamental physics and its applications, *Japanese Journal of Applied Physics* 51 (1R), 010113 (2011).
- [25] S. Kindness, *et al.*, Graphene-Integrated Metamaterial Device for All Electrical Polarization Control of Terahertz Quantum Cascade Lasers. *ACS Photonics* 2019, 6 (6), 1547–1555.
- [26] S. Kalhor, *et al.*, On-chip Superconducting THz Metamaterial Bandpass Filter, *2020 45th International Conference on Infrared, Millimeter, and Terahertz Waves (IRMMW-THz)*, DOI: 10.1109/IRMMW-THz46771.2020.9370663.
- [27] J. Keller, *et al.*, High T_c Superconducting THz Metamaterial for Ultrastrong Coupling in a Magnetic Field, *ACS Photonics* 2018, 5, 10, 3977–3983.
- [28] Y. Xiong, *et al.*, Engineering the Cavity modes and Polarization in Integrated Superconducting Coherent Terahertz Emitters, *2020 45th International Conference on Infrared, Millimeter, and Terahertz Waves (IRMMW-THz)*, DOI: 10.1109/IRMMW-THz46771.2020.9370587.
- [29] S. Kindness, *et al.*, Terahertz Chiral Metamaterial Modulator. *Adv. Opt. Mater.* 2020, 8 (21), 2000581.
- [30] DP Cerkoney, *et al.*, Cavity mode enhancement of terahertz emission from equilateral triangular microstrip antennas of the high-T_c superconductor Bi₂Sr₂CaCu₂O_{8+δ}, *Journal of Physics: Condensed Matter* 29 (1), 015601 (2016).
- [31] Y. Jeong, *et al.*, Dynamic Terahertz Plasmonics Enabled by Phase-Change Materials, *Adv. Optical Mater.* 2020, 8, 1900548
- [32] K. Kadowaki, *et al.*, Quantum terahertz electronics (QTE) using coherent radiation from high temperature superconducting Bi₂Sr₂CaCu₂O_{8+δ} intrinsic Josephson junctions, *Physica C: Superconductivity* 491, 2-6 (2013).
- [33] KHA Villegas, *et al.*, Optical transistor for amplification of radiation in a broadband terahertz domain, *Phys. Rev. Lett.* 124 (8), 087701 (2020)
- [34] K Hayama, Mutual Synchronization of Terahertz Emissions from Multiple Intrinsic Josephson Junction Mesas, *2020 International Conference on UK-China Emerging Technologies (UCET)*, DOI: 10.1109/UCET51115.2020.9205454
- [35] M Tsujimoto, *et al.*, Broadly tunable subterahertz emission from internal branches of the current-voltage characteristics of superconducting Bi₂Sr₂CaCu₂O_{8+δ} single crystals, *Phys. Rev. Lett.* 108 (10), 107006 (2012).
- [36] B. Chen, *et al.*, Hybrid Photon–Plasmon Coupling and Ultrafast Control of Nanoantennas on a Silicon Photonic Chip, *Nano Lett.* 2018, 18, 1, 610–617.
- [37] A. Karabchevsky, *et al.*, On-chip nanophotonics and future challenges, *Nanophotonics* 2020; 9(12): 3733–3753.

- [38] D.-K. Qing and G. Chen, Enhancement of evanescent waves in waveguides using metamaterials of negative permittivity and permeability, *Appl. Phys. Lett.*, 84, 5, 669–671, 2004.
- [39] A. V. Kildishev, *et al.*, Planar photonics with metasurfaces, *Science*, 339, 6125, 1232009, 2013.
- [40] N. Engheta and R. W. Ziolkowski, *Metamaterials: Physics and Engineering Explorations*, Hoboken, NJ, John Wiley & Sons, 2006.
- [41] C. T. Phare, *et al.*, Graphene electro-optic modulator with 30 GHz bandwidth, *Nat. Photonics*, 9, 8, 511–514, 2015.
- [42] M. Delaney, *et al.*, Nonvolatile programmable silicon photonics using an ultralow-loss Sb_2Se_3 phase change material, *Science Advances* 16 Jun 2021: 7, 25, eabg3500 DOI: 10.1126/sciadv.abg3500
- [43] Q. Wang, *et al.*, Optically reconfigurable metasurfaces and photonic devices based on phase change materials, *Nat. Photonics*, 10, 1, 60, 2016.
- [44] M. Liu, *et al.*, A graphene-based broadband optical modulator, *Nature*, 474, 7349, 64–67, 2011.
- [45] L. Chen and E. Towe, Nanowire lasers with distributed-bragg reflector mirrors, *Appl. Phys. Lett.*, 89, 5, 2006,
- [46] S.-W. Ye, *et al.*, High-speed optical phase modulator based on graphene silicon waveguide, *IEEE J. Sel. Top. Quantum Electron.*, 23, 1, 76–80, 2016.
- [47] J. Wang, *et al.*, Integrated photonic quantum technologies, *Nat. Photonics*, 14, 5, 273–284, 2020.
- [48] M. Notomi and T. Sogawa, Nanophotonic technologies for onchip photonic integration, *NTT Technical Rev.*, 16, 7, 7, 2018.
- [49] PR Wiecha, *et al.*, Deep learning in nano-photonics: inverse design and beyond, *Photonics Research* 9 (5), B182-B200, 2021.
- [50] PR Wiecha, OL Muskens, Deep learning meets nanophotonics: a generalized accurate predictor for near fields and far fields of arbitrary 3D nanostructures, *Nano letters* 20 (1), 329-338 (2019).
- [51] O. Kahl, *et al.*, Waveguide integrated superconducting single-photon detectors with high internal quantum efficiency at telecom wavelengths, *Sci. Rep.*, 5, 10941, 2015.
- [52] T. Gerrits, *et al.*, On-chip, photonnumber-resolving, telecommunication-band detectors for scalable photonic information processing, *Phys. Rev. A*, 84, 6, 2011, 060301.
- [53] RH Hadfield, Superfast photon counting, *Nature Photonics* 14 (4), 201-202, 2020.
- [54] S Steinhauer, *et al.*, Progress on large-scale superconducting nanowire single-photon detectors, *Applied Physics Letters* 118 (10), 100501, 2021.
- [55] GJ Orchin, *et al.*, Niobium diselenide superconducting photodetectors, *Applied Physics Letters* 114 (25), 251103, 2019.
- [56] B. Korzh, *et al.*, Demonstration of sub-3 ps temporal resolution with a superconducting nanowire single-photon detector, *Nature Photonics*, 14, 250–255 (2020).
- [57] R. Singh and N. Zheludev, Superconductor photonics, *Nat. Photonics* 8, 679 (2014).
- [58] A. Tsiatmas, *et al.*, Low-loss terahertz superconducting plasmonics, *New J. Phys.* 14, 115006 (2012).
- [59] V.A. Fedotov, *et al.*, Temperature control of Fano resonances and transmission in superconducting metamaterials, *Opt. Express* 18, 9015 (2010).
- [60] R. Singh, *et al.*, Optical tuning and ultrafast dynamics of high-temperature superconducting terahertz metamaterials, *Nanophotonics* 1 (2012): 117–123.